Supporting Information

Changes of phonon modes and electron transfer induced by interface interactions of Pd/MoS_2 heterostructures

Xinyi Chen[1,#], Liang Zhou[1,#], Yusong Wu[1], Yadi Cao[1], Wengui Jiang[1], Yingying Xu[1], Rongming Wang[1,*], Yinghui Sun[1,*]

[1]Beijing Key Laboratory for Magneto-Photoelectrical Composite and Interface Science, The State Key Laboratory for Advanced Metals and Materials, School of Mathematics and Physics, University of Science and Technology Beijing, Beijing 100083, China

Address correspondence to R. M. Wang, E-mail: rmwang@ustb.edu.cn; Y. H. Sun, E-mail: yhsun@ustb.edu.cn

1. Characterizations of the MoS_2 flake before and after transfer

The optical image of a mechanically-exfoliated MoS_2 flake on SiO_2/Si substrate is shown in the inset of Figure S1a. Raman spectrum of the thinner layer of MoS_2 in Figure S1a displays the A_{1g} and E^1_{2g} modes, with an interval of 24.3 cm^{-1}. Combined with the optical contrast of the MoS_2 flake on the SiO_2/Si substrate, it can be determined as a four-layer (4L) MoS_2. Subsequently, the MoS_2 flake was transferred onto a gold microgrid coated with a holey carbon film. As shown in Figure S1b, the surface of the MoS_2 flake after transfer appears quite clean.

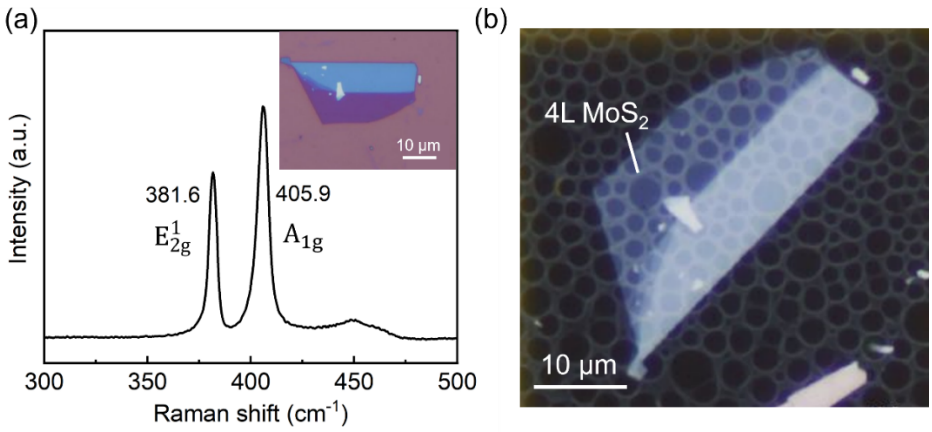

Figure S1. (a) Raman spectrum of the thinner layer of MoS_2. Inset: Optical image of a MoS_2 flake on SiO_2/Si substrate. Raman spectrum was captured from the thinner layer (purple color). (b) Optical image of the MoS_2 flake transferred on gold microgrid coated with a holey carbon film.

2. Schematic diagram and HRTEM image of Pd NPs/MoS_2 heterostructure on TEM microgrid

Figure S2a illustrates the schematic diagram of Pd NPs deposited on the MoS_2 flake on a gold TEM microgrid. HRTEM image in Figure S2b exhibits the typical striped moiré patterns. Figure S2c shows the fast Fourier transform (FFT) pattern of the

region marked by the red dashed frame in Figure S2b. Verified by the reciprocal vector difference formula, the moiré patterns emerge due to the superposition of the two crystal planes of $(202)_{Pd}$ and $(11\bar{2}0)^{MoS_2}$. Furthermore, the expansion of the diffraction spots near the central spot reflects the rotational angle between the moiré fringes and the lattice plane of $(11\bar{2}0)^{MoS_2}$. The included angle between the two orange dashed lines is measured to be 47.4°, indicating that the rotation angles distribute within a range of ±23.7°.

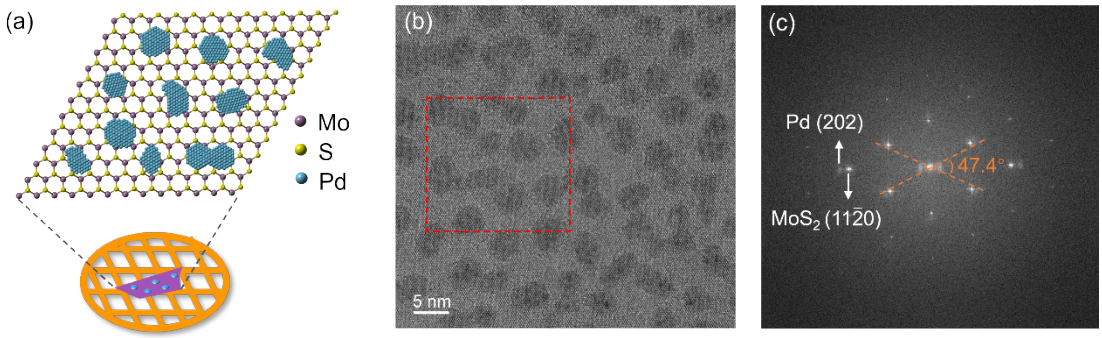

Figure S2. (a) The schematic of Pd NPs/MoS_2 heterostructure on a gold TEM microgrid. (b) HRTEM image of Pd NPs/MoS_2 heterostructure with moiré fringes. (c) Fast Fourier transform (FFT) pattern obtained from the region marked by the red dashed frame in (b). The expansion of the diffraction spots near the central spot reflects the distribution of the rotation angles. The included angle between the two orange dashed lines is measured to be 47.4°.

3. The proportion of element components in Pd/MoS_2 heterostructure

Table S1 shows the atomic number proportions of S, Pd, and Mo elements in Pd/MoS_2 heterostructure, respectively.

Table S1 The proportion of element components in Pd/MoS_2 heterostructure.

element	Line type	Kappa factor	Atomic percentage
S	K	0.586	46.15
Mo	L	1.059	23.59
Pd	L	1.077	30.26
Sum			100.00

4. Raman intensity mapping of A_{1g} and A_{1g}' modes

The Raman intensity mapping was performed on a monolayer MoS_2 domain grown by CVD and deposited with Pd NPs. Figure S3a shows the optical image of the CVD-grown monolayer MoS_2 domain transferred on SiO_2/Si substrate. The white dashed frame indicates the measurement region of Raman mapping. Figures S3b and S3c show the Raman intensity mapping of A_{1g} and A_{1g}' peaks at about 405 and 419 cm^{-1}, respectively. The regions with stronger intensity (larger brightness) correspond to the MoS_2 area within the white dashed frame in Figure S3a, while the dark regions corresponding to the surface of SiO_2/Si substrate. The Raman intensity of A_{1g}' mode is distinctly lower than that of A_{1g} mode, therefore, the Raman intensity mapping of A_{1g}' peak is relatively dimmer (Figure S3c). However, it is noted that the A_{1g}' peak can

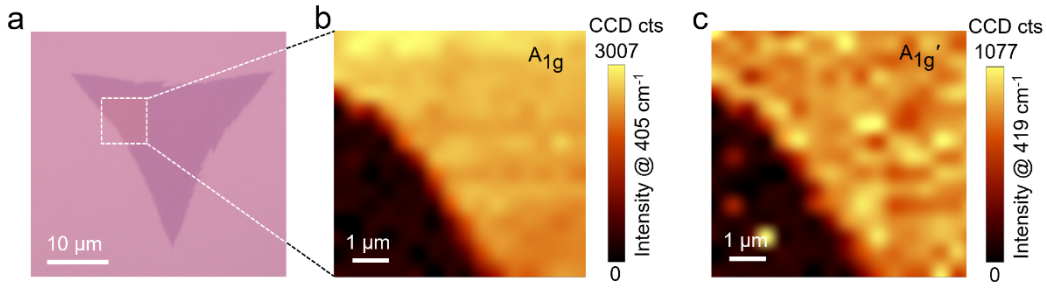

be detected on the whole Pd-MoS_2 area.

Figure S3. (a) Optical image of a CVD-grown monolayer MoS_2 domain transferred on SiO_2/Si substrate. The white dashed frame indicates the measurement region of Raman mapping. (b, c) Raman mapping of the intensity of A_{1g} and A_{1g}' peaks, respectively.

5. Raman spectra of defect-rich MoS_2

To exclude the possibility of the defects in MoS_2 inducing the new vibration mode, the defect-rich MoS_2 was obtained by air plasma treatment on few-layer MoS_2 flake for 25 s. The comparison of Raman spectra before and after the plasma treatment in Figure S4 exhibits the broadened Raman peaks of E_{2g}^1 and A_{1g} modes after the plasma treatment, rather than the emergence of any new phonon mode.

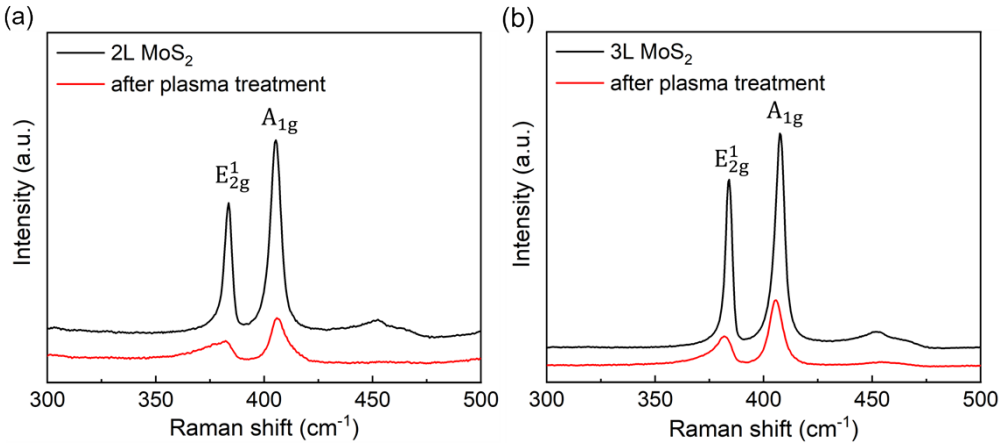

Figure S4. Raman spectra of 2L (a) and 3L (b) MoS_2 before and after air plasma treatment.

6. Optical images of exfoliated MoS_2 flakes and CVD-MoS_2 domains on SiO_2/Si substrate

The optical images in Figure S5a-b clearly show that the distribution of CVD-MoS_2 domains is denser with higher coverage on the substrate, compared with the exfoliated MoS_2 flakes.

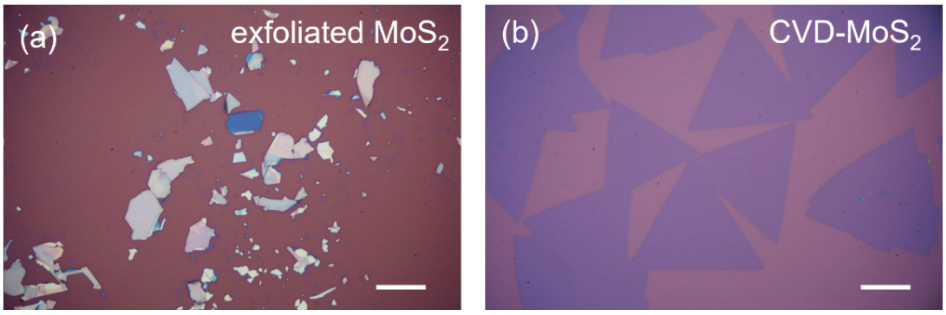

Figure S5. Optical images of mechanically exfoliated MoS_2 flakes (a) and monolayer MoS_2 domains grown by chemical vapor deposition (CVD) (b) on SiO_2/Si substrate. The scale bars are all 20 μm.

7. Differential charge density between monolayer MoS_2 and Pd atoms

The differential charge density between monolayer MoS_2 and Pd atoms was calculated by employing the Vienna ab initio simulation package (VASP) based on density functional theory (DFT). Theoretical calculations reveal the charge transfer between Pd atoms and MoS_2. Pd diatom transfer 0.28 electrons to MoS_2, with an average of 0.14 electrons transferred from per Pd atom (Figure S6a). Pd triatom transfer 0.33 electrons to MoS_2, with an average of 0.11 electrons transferred from per Pd atom (Figure S6b).

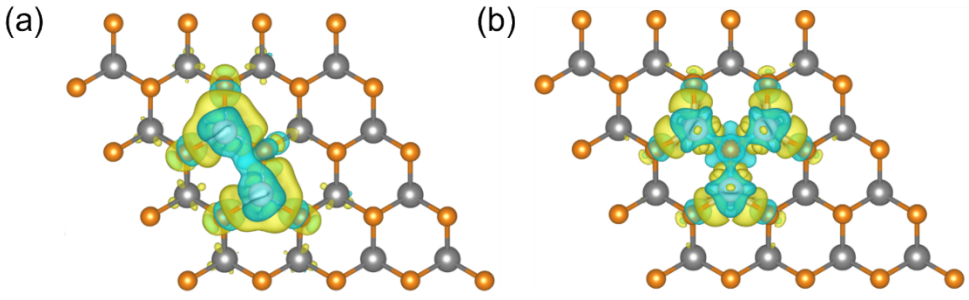

Figure S6. Differential charge density of Pd diatom-MoS_2 (a) and Pd triatom-MoS_2 (b) (top view). Yellow color marks the charge accumulation and blue color marks the charge depletion, respectively.

8. Fabrication process of Pd/MoS_2 heterostructure inserted with graphene

A dry transfer method was used to prepare graphene/MoS_2 heterostructure with a clean interface. Figure S7 shows the schematic diagram of the fabrication process of graphene transferred onto MoS_2 flake with the subsequent deposition of Pd NPs.

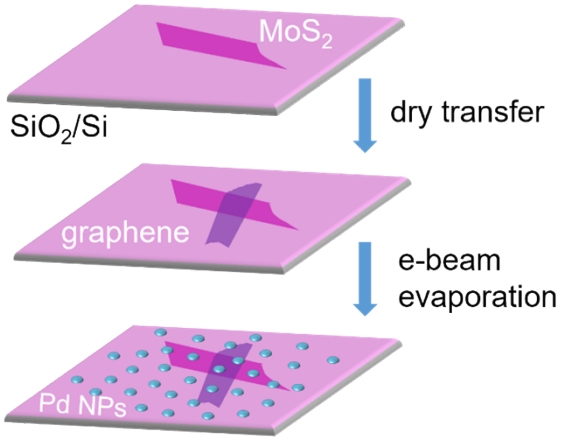

Figure S7. Schematic diagram of the preparation process of Pd NPs/graphene/MoS_2 heterostructure.